Int. J. Heat Mass Transfer. Vol. 34, No. 8, pp. 2039–2051, 1991
Printed in Great Britain

0017–9310/91 $3.00 + 0.00

Unsteady three-dimensional mixed convection in a heated horizontal channel with applications to chemical vapor deposition

GREG EVANS
Computational Mechanics Division, Sandia National Laboratories, Livermore, CA 94550, U.S.A.

and

RALPH GREIF
Mechanical Engineering Department, University of California, Berkeley, CA 94720, U.S.A.

(*Received* 28 *December* 1989 *and in final form* 2 *October* 1990)

Abstract—The flow and heat transfer of a gas in a horizontal channel with a heated bottom surface, a cooled top surface, and adiabatic side walls is studied. Numerical solutions of the transient, three-dimensional Navier–Stokes and energy equations reveal that the fluid is unstable thermally for conditions of interest in chemical vapor deposition (CVD). The instability appears as a combination of transverse, traveling waves and longitudinal rolls. The unsteady nature of the flow and the heat transfer is shown for two Reynolds numbers, $Re = \bar{u}H/\nu_0$ (5 and 10), Grashof number, $Gr = g\varepsilon H^3/\nu_0^2 = 5000$, Prandtl number, $Pr = \nu_0/\alpha_0 = 2/3$, aspect ratios, $L/H = 8$ and $W/H = 2$, for the temperature ratio $\varepsilon = (T_s - T_0)/T_0 = 0.01$, corresponding to constant property flow. The instability results in an increase in the average heat transfer from 15% to more than 40% above the fully developed condition in the absence of the instability.

INTRODUCTION

CHEMICAL vapor deposition (CVD) is an important process for fabricating micro-electronic components. Although widely used, the CVD process is not very well understood and empirical methods are often used for reactor design and for setting reactor operating conditions. In the CVD process, a mixture of reacting and inert gases, e.g. silane and helium, flows over a heated substrate. Upon heating, the reactant gases pyrolyze to form additional species that are transported to the heated substrate where surface reactions produce a solid deposit, e.g. silicon. Several parameters can be controlled; e.g. reactor geometry, gas flow rates and flow rate distributions, thermal boundary conditions on reactor surfaces, reactant gas composition, etc. Some important quantities of interest in the fabrication of semiconductors with CVD are the rate and the uniformity of the deposition, and the sharpness of the interfaces between adjacent layers.

Fluid flow and convective heat transfer are important factors in the CVD process as noted by Jensen [1], Giling [2], Coltrin *et al.* [3], Ostrach [4], and Curtis and Dismukes [5], with buoyancy effects being significant in many cases. Recirculation regions can result in increased purge times of reactive gases and can have a detrimental effect on the sharpness of interfaces between layers in semiconductor processing by CVD. If the deposition process is controlled by mass transport to the surface, the presence of boundary layers can adversely affect the uniformity of the solid being deposited and can result in a reduced rate of deposition. Thermally unstable secondary flows can result in significantly higher deposition rates; however, if the secondary flow is steady the uniformity of the deposit can be impacted adversely. On the other hand, unstable, transient flows that sweep periodically through the reactor can result in uniform deposition in conjunction with significantly higher deposition rates.

In general, the prediction of deposition rates and distributions in a CVD reactor would require the solution of the three-dimensional, time-dependent conservation equations of mass, momentum, and energy in the reactor geometry of interest with specified boundary conditions. In addition, chemical reaction mechanisms are required to describe the gas phase and the surface chemistry, and constitutive relations must be specified for the shear stress, heat flux, and mass diffusion flux. The complete solution of CVD problems is not feasible at present; however, for some conditions and reactor geometries, CVD processes can be simplified to one-dimensional or two-dimensional (boundary layer) formulations (cf. Coltrin *et al.* [3]; Pollard and Newman [6]; Coltrin *et al.* [7]). Some three-dimensional aspects of CVD have recently been studied (cf. Cullen [8]). Moffat and Jensen [9, 10] solved the steady-state, parabolized heat, momentum, and mass-transfer equations for variable property, mixed convection in a horizontal channel. They included finite rate chemistry in the dilute reactant formulation which is discussed below.

In many CVD problems the fluid mechanics and heat transfer can be separated from the chemistry and species transport. The reactants often appear as trace species in an inert carrier gas; consequently predictions of the flow field and the heat transfer can be

NOMENCLATURE

c	speed of sound
c_p	dimensionless specific heat
D	substantial derivative
f	dimensionless frequency, $1/t$
g	acceleration of gravity
Gr	Grashof number, $g\varepsilon H^3/\nu_0^2$
H	channel height
k	dimensionless thermal conductivity
L	channel length
n_i	unit gravitational vector
$Nu_{l,u}$	local Nusselt numbers on bottom and top surfaces, $q^*_{l,u}H/k_0(T_s-T_0) = -k(\partial\Theta/\partial y)\|_{y=0,1}$
$\overline{Nu}_{l,u}$	average Nusselt numbers on bottom and top surfaces, $\overline{q^*_{l,u}}H/k_0(T_s-T_0) = (H^2/WL)\Sigma_{l,u}Nu_{l,u}\,\Delta x\,\Delta z$
p	dimensionless pressure
$\hat{p}$	dimensionless pressure due to motion in momentum equations
Pr	Prandtl number, $\nu_0/\alpha_0 = 2/3$ for helium
P_u	power spectrum of axial velocity oscillations
$q^*_{l,u}$	dimensional local heat flux at bottom and top surfaces, $-k^*(\partial T/\partial y^*)\|_{y^*=0,H}$
$\overline{q^*_{l,u}}$	dimensional average heat flux at bottom and top surfaces, $Q^*_{l,u}/(WL)$
$Q^*_{l,u}$	total dimensional heat flow rate from bottom and top surfaces, $\Sigma_{l,u}q^*_{l,u}\,\Delta x^*\,\Delta z^*$
Ra	Rayleigh number, $g\varepsilon H^3/(\nu_0\alpha_0) = Gr\,Pr$
Re	Reynolds number, $\bar{u}H/\nu_0$
t	dimensionless time
T	dimensional temperature
u	dimensionless axial velocity
$\bar{u}$	average dimensional axial velocity at inlet of channel
v	dimensionless vertical velocity
w	dimensionless spanwise velocity
W	channel width
x	dimensionless axial coordinate
Δx	dimensionless grid spacing in axial direction
y	dimensionless vertical coordinate
z	dimensionless spanwise coordinate
Δz	dimensionless grid spacing in spanwise direction.

Greek symbols

α	thermal diffusivity
β	dimensional coefficient of thermal expansion, $1/T_0$
δ_{ij}	Kronecker delta
ε	temperature ratio, $(T_s-T_0)/T_0$
Θ	dimensionless temperature, $(T-T_0)/(T_s-T_0)$
μ	dimensionless dynamic viscosity
ν	dimensionless kinematic viscosity
ρ	dimensionless density.

Subscripts and superscripts

s	conditions at hot surface of channel ($y = 0$)
0	dimensional quantities evaluated at temperature T_0 and to conditions at cold surface of channel ($y = 1$)
*	dimensional quantity.

made by solving conservation equations for a single species. Furthermore, the deposition is often limited by convection and diffusion processes in the gas phase [11, 12], and for those situations in which the analogy between heat and mass transfer is valid, the uniformity and magnitude of the deposit can be obtained directly from the solution of the energy equation for the carrier gas. If the analogy cannot be made, then the species equations must also be solved to obtain the deposition rates.

THE HORIZONTAL CHANNEL FLOW REACTOR

An idealized horizontal channel flow reactor is shown in Fig. 1. The channel height, H, is usually a few centimeters, the channel length, L, is approximately 1 m, and the width, W, is approximately 10 cm. Although not shown in Fig. 1, an unheated entrance length may be present to allow for hydrodynamic development of the flow. A heated substrate, $T_s \approx$

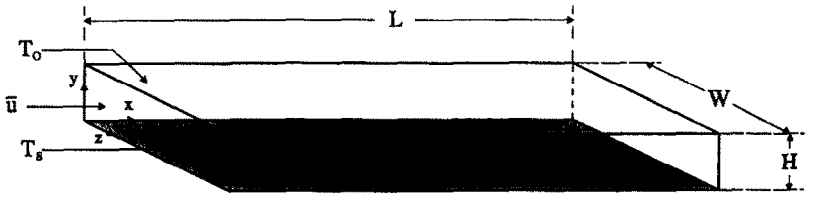

FIG. 1. Horizontal channel reactor geometry and coordinate system.

1000–1300 K, which is several centimeters to several tens of centimeters in length, forms the lower surface of the channel. The carrier gas is usually hydrogen or an inert gas such as helium, argon, or nitrogen. At the channel inlet, the average flow velocity, $\bar{u}$, is a few centimeters per second. The Reynolds number, $Re = \bar{u}H/\nu_0$, and Mach number, $\bar{u}/c$, of these flows are small ($Re \approx 1$–100, $Ma \ll 1$). The Grashof number, $Gr = g\varepsilon H^3/\nu_0^2$, is between 10^3 and 10^5. The density and other properties undergo significant changes due to the large temperature differences and the Boussinesq approximation (density constant everywhere except in the body force term) is not normally valid.

The relative effects of inertia and buoyancy appear in the ratio: Re^2/Gr. Values of this ratio that are typical in CVD (10^{-3}–10^{-1}) have been shown (cf. below) to result in significant buoyancy effects. Secondary flow instabilities can occur varying from transverse, traveling waves that are oriented at right angles to the main flow to steady, longitudinal rolls that are aligned with the main flow. In both cases the heat transfer rate from the substrate to the gas is increased significantly (when the instability is present), and hence the deposition rate would also be increased. However, for the transverse waves the instability sweeps through the channel at a rate that is related to the value of Re^2/Gr whereas with longitudinal rolls the instability remains stationary. Thus, these instabilities would be expected to produce dramatically different effects on the uniformity and thickness of the deposited material.

Summary of related research

Mori and Uchida [13] performed a linearized stability analysis of fully developed flow in a horizontal channel heated from below and predicted an instability consisting of steady longitudinal rolls for $Ra > 1708$. Their disturbances were assumed to be steady and periodic in the spanwise direction only. Experiments confirmed this roll structure and increased heat transfer for $Re^2/Gr > 10$.

Gage and Reid [14], in a three-dimensional time-dependent stability analysis of the linearized equations for thermally stratified plane Poiseuille flow of infinite horizontal extent, also found that the flow was unstable for Rayleigh numbers greater than 1708 ($Ra = g\varepsilon H^3/(\nu_0\alpha_0) = Gr\,Pr$, where Pr is the Prandtl number; Gage and Reid considered only the $Pr = 1$ case). Although the occurrence of a longitudinal roll instability (axis aligned with the main flow) was independent of the value of Re, other flow instabilities were allowed including traveling transverse waves (axis perpendicular to the main flow direction) depending on the relative values of Re and Ra.

Akiyama *et al.* [15] used flow visualization and temperature measurements to verify thermal instability in the fully developed flow of air in a horizontal channel heated from below for $Ra > 1708$. Evidence of longitudinal structures was apparent for values of Re^2/Gr as small as 0.007.

Ostrach and Kamotani [16] measured the heat transfer and temperature profiles in fully developed mixed convection of air in horizontal channel flow between isothermal plates (lower surface hotter). They determined that for $10 < Re < 100$, $Ra < 8000$ the flow consisted of well-developed longitudinal rolls. Later studies [17] were performed for larger Ra in the thermally developing region of the flow that showed mushroom shaped thermals impinging on the upper surface with noticeable upstream disturbances for $Re^2/Gr < 0.1$.

Incropera *et al.* [18] studied mixed convection in horizontal channels for constant heat flux conditions and determined that the flow pattern contained ascending thermals that developed into mushroom shaped longitudinal vortices. The instability became time dependent at large downstream distances with the heat transfer being characterized by turbulent natural convection.

Platten and Legros [19] performed an analytical investigation of buoyant convection in horizontal channel flows of finite lateral extent. They determined the values of the Rayleigh and Reynolds numbers yielding traveling transverse waves. In an experimental study, Luijkx *et al.* [20] demonstrated the existence of traveling transverse waves in a channel of lateral aspect ratio, $W/H = 5$, that was heated from below and cooled from above with a fully developed Poiseuille velocity profile for the initial condition. As the Reynolds number was increased, the transverse waves were eventually replaced by longitudinal rolls.

Chiu and Rosenberger [21] determined experimentally the thermal entry lengths for the onset of instability and the development of the flow of nitrogen in a horizontal channel with an inlet parabolic flow profile for $1368 < Ra < 8300$ and $15 < Re < 170$ and $W/H = 10$. They observed steady longitudinal rolls for $Re^2/Gr = 0.3$; however, for large Ra and small Re ($Re^2/Gr \approx 0.03$), they noted that the longitudinal rolls were unsteady and indicated that this was due to a combination of traveling transverse waves and longitudinal rolls.

Recently, transient two-dimensional mixed convection in a horizontal channel was studied numerically and traveling transverse waves for values of Re^2/Gr ranging from 10^{-3} to 10^{-1} were predicted [22, 23].

Moffat and Jensen [9, 10] solved the steady, three-dimensional parabolized Navier–Stokes equations numerically for variable property mixed convection flow in a horizontal channel ($W/H = 4$, $L/H = 10$) for $Re = 64$, $Gr = 1.87 \times 10^5$ ($Re^2/Gr = 0.022$). The resulting flow patterns consisted of steady, longitudinal rolls.

The previous studies have shown that traveling transverse waves occur in a channel flow that is heated from below when Ra is greater than a critical value and Re is sufficiently small. As Re^2/Gr is increased much above 0.1 (for $Pr \approx 1$), the traveling transverse waves are replaced by longitudinal rolls. For very

large values of Re^2/Gr, the flow is dominated by forced convection. It is emphasized that the values of Re^2/Gr that occur in CVD cover the range of parameters that include both traveling transverse waves and longitudinal rolls.

We have investigated the three-dimensional transient mixed convection flow in an idealized horizontal channel CVD reactor that is heated from below and cooled from above (cf. Fig. 1). We have determined that the flow patterns are complex and time dependent and consist of both traveling transverse waves and spanwise recirculating regions.

GOVERNING EQUATIONS

The conservation equations for a fluid continuum are valid for most CVD applications even when the pressure in the system is only a few Torr. However, at these low pressures, the assumption that the fluid flow and the heat transfer in the carrier gas are separable from the reacting species is no longer valid because the reacting species now form a large fraction of the gas in the system. Thus, the applicability of the present results to CVD is limited to situations when the carrier gas is the dominant species.

The geometry is shown in Fig. 1. The equations are made dimensionless with channel height H, buoyant velocity $\sqrt{(g\varepsilon H)}$, time $\sqrt{(H/(g\varepsilon))}$, pressure $\rho_0 g\varepsilon H$, and temperature difference $T_s - T_0$ with $\Theta = (T-T_0)/(T_s-T_0)$, where T_s and T_0 are the temperatures of the lower and upper surfaces of the channel, respectively. The fluid properties are made dimensionless with the values evaluated at the temperature T_0, designated by the subscript '0'. We emphasize that the Boussinesq approximation is not invoked. The dimensionless equations for an ideal gas are

$$\frac{\partial \rho}{\partial t} + \frac{\partial(\rho u_j)}{\partial x_j} = 0 \tag{1}$$

$$\frac{\partial(\rho u_i)}{\partial t} + \frac{\partial}{\partial x_j}(\rho u_i u_j) = -\frac{\partial \hat{p}}{\partial x_i} + \frac{(\rho - 1)}{\varepsilon} n_i + Gr^{-1/2}\frac{\partial \tau_{ij}}{\partial x_j} \tag{2}$$

$$\frac{\partial(\rho\Theta)}{\partial t} + \frac{\partial}{\partial x_j}(\rho u_j \Theta) = Gr^{-1/2} Pr^{-1}\left[\frac{\partial}{\partial x_j}\left(\frac{k}{c_p}\frac{\partial \Theta}{\partial x_j}\right) + \frac{k}{c_p^2}\frac{\partial \Theta}{\partial x_j}\frac{\partial c_p}{\partial x_j}\right] \tag{3}$$

$$\rho = \frac{\rho_s}{\rho_s(1-\Theta)+\Theta} \tag{4}$$

where

$$x_i = (x, y, z); \quad \tau_{ij} = \mu\left(\frac{\partial u_i}{\partial x_j} + \frac{\partial u_j}{\partial x_i}\right) - \frac{2}{3}\delta_{ij}\mu\frac{\partial u_k}{\partial x_k};$$

$$\varepsilon = (T_s - T_0)/T_0.$$

In equations (2) and (4) we have utilized the results of a small Mach number expansion of the pressure [24] which is also discussed in ref. [23]. The hydrostatic component of the pressure and the body force are included in the second term on the right-hand side of equation (2) where n_i is the unit gravitational vector. In the energy equation (3), viscous dissipation and compressibility effects associated with Dp/Dt are ignored and the Prandtl number Pr is defined as ν_0/α_0. In equation (4) ρ_s is the dimensionless gas density, evaluated at the temperature of the heated lower surface.

We restrict the analysis to the following conditions: $L/H = 8$; $W/H = 2$; fully developed velocity profile initially and at the channel entrance (at $x = 0$); adiabatic side walls (at $z = 0, 2$); small temperature differences ($\varepsilon = 0.01$) corresponding approximately to constant property conditions; helium gas ($Pr = 2/3$); and a temperature profile that varies linearly from the bottom to the top of the channel is applied initially and at the channel entrance. Although as noted earlier, most CVD conditions do not correspond to the constant property situation, we choose in this work to focus on the combined effects of buoyancy and forced convection flow and not on the variation of transport properties. We have made preliminary calculations with variable properties for helium and the results are qualitatively similar. Specifically, the initial and boundary conditions are:

at $t = 0$

$$u = 6(Re/Gr^{1/2})\left\{ y - y^2 - \sum_{n=1,3,5,\ldots} \frac{8\cosh\left[n\pi\left(z - \frac{w}{2H}\right)\right]\sin(n\pi y)}{(n\pi)^3 \cosh\left(n\pi\frac{w}{2H}\right)} \right\},$$

$$v = 0, \quad \Theta = 1 - y,$$

$$\text{for} \quad 0 \leqslant x \leqslant L/H, \quad 0 \leqslant y \leqslant 1, \quad 0 \leqslant z \leqslant W/H; \tag{5}$$

for $t > 0$

$$u = 6(Re/Gr^{1/2})\left\{ y - y^2 - \sum_{n=1,3,5,\ldots} \frac{8\cosh\left[n\pi\left(z - \frac{w}{2H}\right)\right]\sin(n\pi y)}{(n\pi)^3 \cosh\left(n\pi\frac{w}{2H}\right)} \right\},$$

$$v = 0, \quad \Theta = 1 - y,$$

$$\text{for} \quad x = 0, \quad 0 \leqslant y \leqslant 1, \quad 0 \leqslant z \leqslant W/H;$$

$$\frac{\partial u}{\partial x} = \frac{\partial v}{\partial x} = \frac{\partial w}{\partial x} = \frac{\partial \Theta}{\partial x} = 0,$$

$$\text{for} \quad x = L/H, \quad 0 \leqslant y \leqslant 1, \quad 0 \leqslant z \leqslant W/H;$$

$$u = v = w = 0, \quad \Theta = 1,$$

$$\text{for} \quad 0 \leqslant x \leqslant L/H, \quad 0 \leqslant z \leqslant W/H, \quad y = 0;$$

$$u = v = w = \Theta = 0,$$

$$\text{for} \quad 0 \leqslant x \leqslant L/H, \quad 0 \leqslant z \leqslant W/H, \quad y = 1. \quad (6)$$

Note that the velocity scaling has been chosen to analyze flows with small values of Re^2/Gr. The six parameters in the above equations and boundary conditions are: Re, Gr, Pr, ε, L/H, and W/H. The infinite series in the expression for the fully developed u velocity (cf. pp. 150–152 of ref. [19]) in equations (5) and (6) converges quickly (20 terms have been used in the present study).

NUMERICAL SOLUTIONS

Solution method and determination of accuracy

Equations (1)–(4) with initial conditions (5) and boundary conditions (6) are integrated over control volumes and finite differences are used to discretize the derivatives. A central difference formulation is used for all spatial derivatives and a backward Euler method is applied to the time derivatives. The solution method is semi-implicit and is based on the TEACH code (cf. Gosman and Pun [25]). The momentum and energy equations are solved implicitly along lines that are normal to the four channel surfaces and the equation for pressure is solved implicitly along lines both normal and parallel to the channel surfaces in an alternating fashion. The SIMPLER method described by Patankar [26] is used to determine the pressure field. Under-relaxation factors of 0.9 and 0.8 are used in the solution of the momentum and energy equations, respectively. There is no under-relaxation of the pressure equation. At each time step, in order to obtain an accurate transient solution, the equations are iterated until the following convergence criteria are achieved: at each grid point and for each dependent variable, the relative change from one iteration to the next must be less than 1 part in 10^5 and the absolute change must be less than 1 part in 10^6. Once these iteration criteria have been achieved for all of the dependent variables, a check is then made of the relative and absolute changes of all of the dependent variables at all of the grid points from the preceding time to the current time. If any variable at any grid point changes by more than 10% between time steps, the result is rejected, the current value of the time step is halved and the computation is repeated for the new current time. The residuals of the equations (absolute values summed over the grid and normalized by the number of control volumes) are also checked and typical values at convergence are between 10^{-4} and 10^{-5}. Global energy and momentum balances are maintained to better than 1% at each time step.

The sensitivity of the results to the grid size and the time step have been obtained. As an example, for the case $Re = 5$, $Gr = 5000$, the changes in the local and average Nusselt numbers on the lower and upper surfaces of the channel when the number of x grid points was increased from 81 to 101 was less than 1%. Similar changes occurred when the number of z grid points was increased from 21 to 32, and when the number of y grid points was reduced from 21 to 15, the changes in the Nusselt numbers were between 2 and 3%. Consequently, for the results presented here, an (x, y, z) grid of (81, 21, 21) points was used. The time step was 0.2; for the above case, results for the average and local Nusselt numbers on the lower and upper surfaces of the channel changed by less than 0.5% when the time step was halved to 0.1.

Results

Equations (1)–(4) with boundary conditions (6) were integrated, starting with the initial conditions (5), until the time average of the spatially averaged Nusselt numbers (defined below) on the lower and upper surfaces of the channel became stationary. We define stationarity to be the condition when the spatially averaged Nusselt numbers change by less than 2% over a time interval that is large compared to the characteristic time of the system. Two cases have been studied in detail to examine the unsteady, three-dimensional interactions between buoyancy and forced flow, namely $Re = 5$ and 10, for $Gr = 5000$, $L/H = 8$, $W/H = 2$, and $\varepsilon = 0.01$ (constant properties). Unsteady variations of the three components of velocity and temperature are plotted at several locations within the channel. Field plots of velocity and temperature as well as variations of the local and average Nusselt numbers are also presented.

In Figs. 2(a)–(c), the temporal variations of the temperature (Θ) and of the velocity components (u, v) in the axial, x, and vertical, y, directions at the center point $(x, y, z) = (4.0, 0.5, 1.0)$, of the channel are shown for $Re = 5$. The oscillations reach a periodic state with Θ and v having the same frequency, $f = 0.032$, in Figs. 2(a) and (b) while u in Fig. 2(c) has a frequency that is twice this value. The amplitudes of the oscillations of Θ and v are constant and symmetrical about 0.5 and 0.0, respectively, whereas that of u varies slightly in a periodic manner. The results are symmetric about the central vertical plane, $z = 1.0$, with the velocity (w) in the transverse (z) direction being essentially zero at $z = 1.0$. Note that the symmetry about $z = 1.0$ has not been assumed. The temporal variation of w in Fig. 3 at the location $(x, y, z) = (4.0, 0.5, 0.47)$ is similar to that of u at the center point (cf. Fig. 2(c)). The temporal variations of Θ, v and u at $(x, y, z) = (4.0, 0.5, 0.47)$ (not shown) are similar although smaller in amplitude in comparison to their respective variations at the center point.

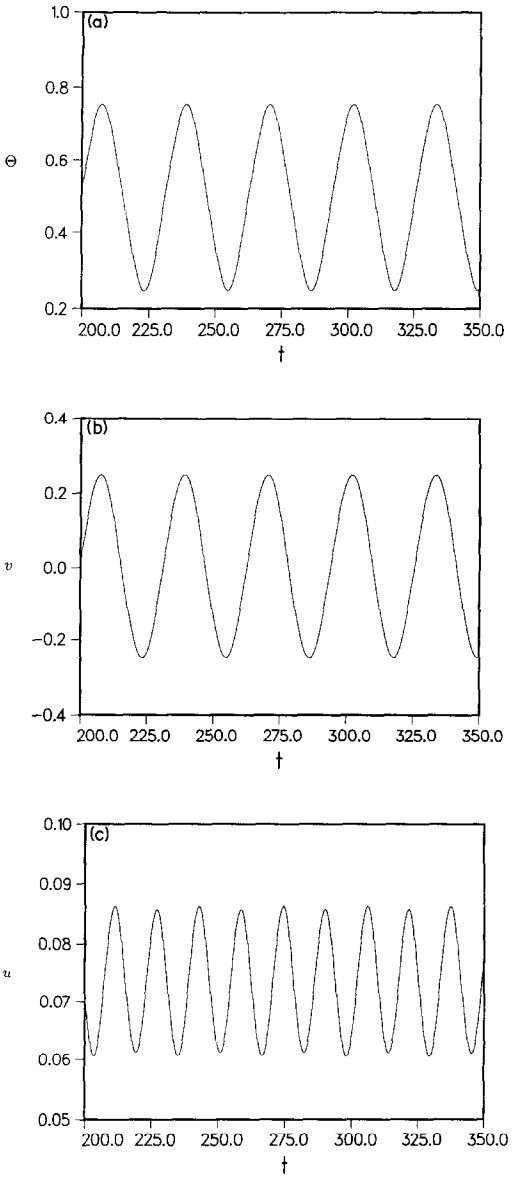

FIG. 2. Temporal oscillations at the center point $(x, y, z) = (4.0, 0.5, 1.0)$ of the channel for $Re = 5$, $Gr = 5000$: (a) temperature, Θ; (b) vertical component of velocity, v; (c) axial component of velocity, u.

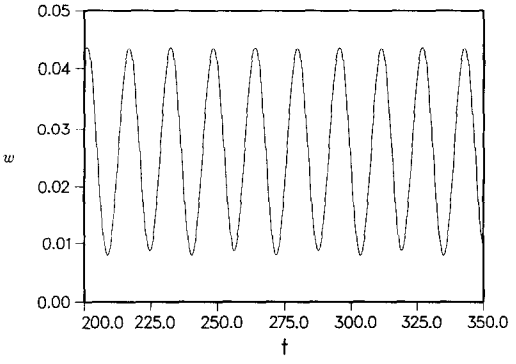

FIG. 3. Temporal oscillations of the spanwise component of velocity, w, at the point $(x, y, z) = (4.0, 0.5, 0.47)$ of the channel for $Re = 5$, $Gr = 5000$.

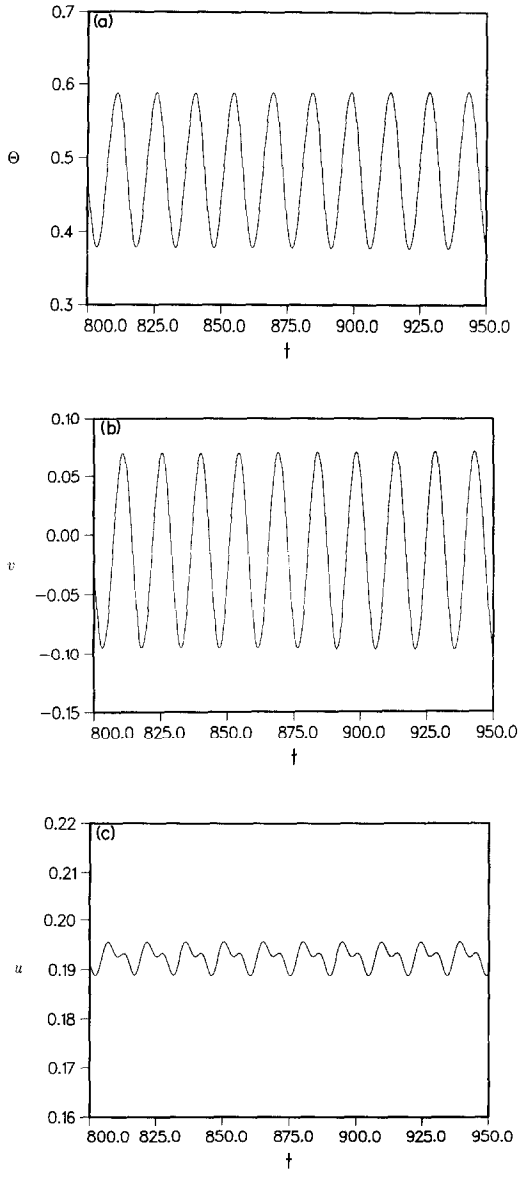

FIG. 4. Temporal oscillations at the center point $(x, y, z) = (4.0, 0.5, 1.0)$ of the channel for $Re = 10$, $Gr = 5000$: (a) temperature, Θ; (b) vertical component of velocity, v; (c) axial component of velocity, u.

Figures 4(a)–(c) show the temporal variations of Θ, v, and u at the center point for $Re = 10$ after the Nusselt numbers have become stationary. Again, periodic oscillations occur; however, now the frequency for Θ and v is significantly higher ($f = 0.068$) and the amplitudes are much smaller than for $Re = 5$ (0.21, 0.17 and 0.007 for Θ, v and u for $Re = 10$ vs 0.51, 0.50 and 0.026 for Θ, v and u for $Re = 5$). The frequency is higher at $Re = 10$ due to the greater relative effect of forced flow which translates the instability down stream at a faster rate. The smaller amplitudes at $Re = 10$ are because the instability has just become established at the center point of the channel whereas for $Re = 5$ it was well established. Recall also that for

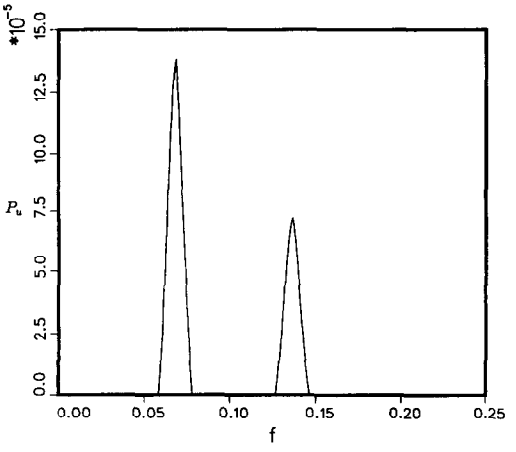

FIG. 5. Power spectrum of oscillations of the axial component of velocity, u, at the center point $(x, y, z) = (4.0, 0.5, 1.0)$ of the channel for $Re = 10$, $Gr = 5000$.

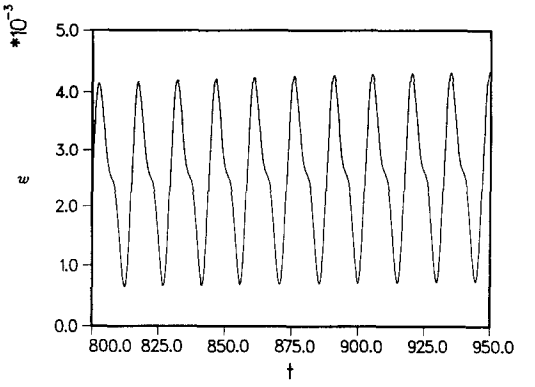

FIG. 6. Temporal oscillations of the spanwise component of velocity, w, at the point $(x, y, z) = (4.0, 0.5, 0.47)$ of the channel for $Re = 10$, $Gr = 5000$.

$Re = 5$ the oscillations of Θ and v are symmetric about 0.5 and 0.0, respectively; however, for $Re = 10$ the average values of Θ and v are now smaller than 0.5 and negative, respectively. This is consistent with a spanwise recirculation where the heated fluid rises near the side walls, is cooled along the top and descends in the middle of the channel, leading at the center to a value of Θ that is smaller than 0.5 and a v velocity that is biased negatively, i.e. downward flow.

The temporal variation of u in Fig. 4(c) shows the same fundamental frequency as for Θ and v in Figs. 4(a) and (b); this differs from $Re = 5$ which showed that the frequency for u was twice that of Θ and v. However, the oscillation at $Re = 10$ is not a single frequency, and a power spectral analysis shown for u in Fig. 5 reveals significant energy content at the second harmonic ($f = 0.136$).

For $Re = 10$, Fig. 6 shows the temporal variation of w off the central plane at $(x, y, z) = (4.0, 0.5, 0.47)$. A spectral analysis shows that all of the variables have the same fundamental frequency at (4.0, 0.5, 0.47) which is also the same at the center (4.0, 0.5, 1.0). The oscillations of Θ and v consist of a single frequency at both locations whereas u and w have significant energy at the second harmonic. Recall that for $Re = 5$ there is little energy content for w at the second harmonic (cf. Fig. 3).

The temperature fields on the vertical central plane, $z = 1.0$, are shown in Fig. 7(a) for $Re = 5$, and in Fig. 7(b) for $Re = 10$. In both cases, the fields are shown at a time ($t = 270.6$ for $Re = 5$ and $t = 869.4$ for $Re = 10$, cf. Figs. 2(a) and 4(a)) of maximum temperature at the center point of the channel. At the higher Re there is an axial delay of the onset of the thermal instability. This delay also occurred in our earlier study of two-dimensional transverse traveling waves in a horizontal channel flow [23].

In Figs. 8(a) and (b), the velocity fields are shown in the spanwise (yz) planes at the two axial locations, $x = (4.0, 5.0)$, for $Re = 5$ at the same time, $t = 270.6$. The flow pattern at $x = 4.0$ and also at $x = 6.0$ (not shown) consists of fluid that is primarily ascending in the yz plane, with only a small z component of velocity near the adiabatic side walls. However, at $x = 5.0$ and also at $x = 7.0$ (not shown), the motion is essentially the opposite, i.e. primarily descending. Note that the

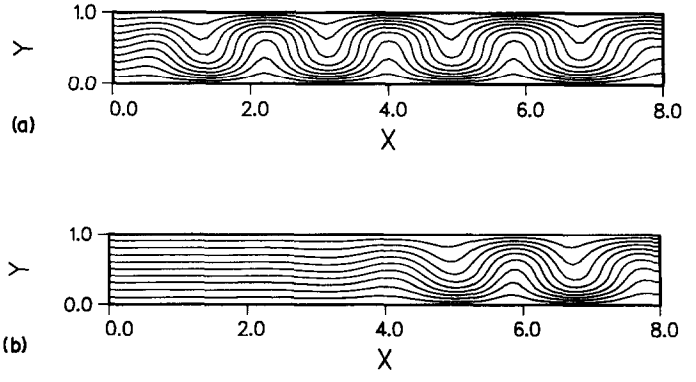

FIG. 7. Temperature fields in the vertical central plane ($z = 1.0$) of the channel at a time of maximum temperature at the center point, $(x, y, z) = (4.0, 0.5, 1.0)$, for $Gr = 5000$: (a) $Re = 5$, $t = 270.6$; (b) $Re = 10$, $t = 869.4$.

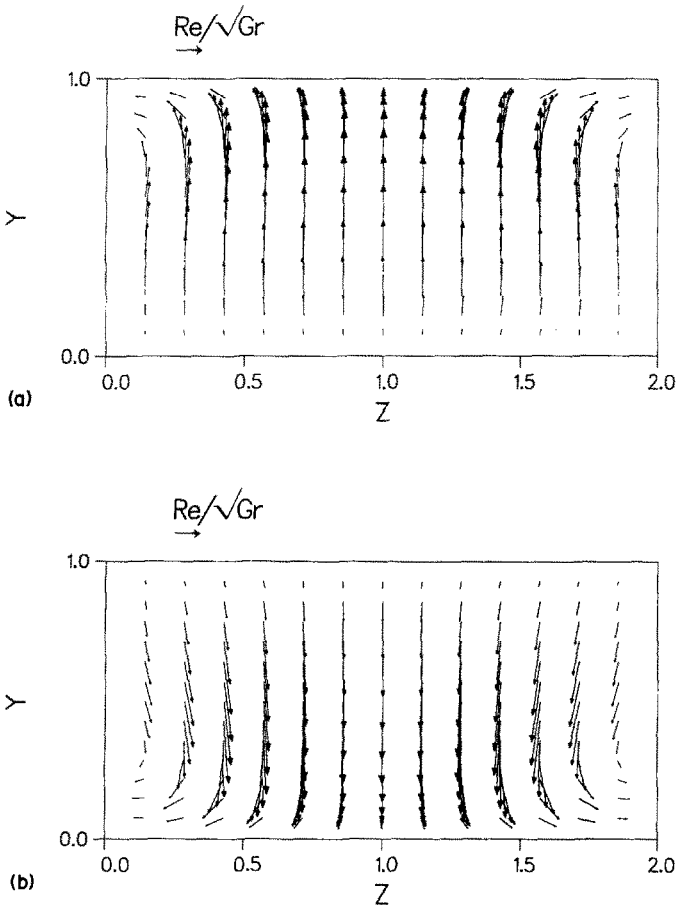

FIG. 8. Velocity fields in spanwise (yz) planes for $Re = 5$, $Gr = 5000$, $t = 270.6$: (a) $x = 4.0$; (b) $x = 5.0$.

locations $x = (4.0, 6.0)$ correspond to positions of crests of the transverse traveling waves as shown in Fig. 7(a) while there are troughs at $x = (5.0, 7.0)$. The velocity vectors in the central xy plane are displayed in Fig. 9 at $t = 270.6$. At a later time, $t = 286.4$, which corresponds to a time of minimum temperature at the center point (one-half period later, cf. Fig. 2(a)), the flow patterns in the yz planes discussed above are exactly reversed (not shown). The exact reversal is consistent with the symmetrical oscillations previously discussed in connection with Figs. 2(a) and (b).

For $Re = 10$ the spanwise (yz) velocity fields are shown in Figs. 10(a) and (b) at $x = 5.0$ for $t = 869.4$ (time of maximum center point temperature) and $t = 876.8$ (time of minimum center point temperature, one-half period later, cf. Fig. 4(a)). In contrast to $Re = 5$ discussed above, the flow patterns now are not exactly reversed. The central downward flow in Fig. 10(a) exhibits a recirculation which is stronger than for upward flow in Fig. 10(b). A similar inexact reversal occurs for these two times at $x = 4.0$. This is consistent with Figs. 4(a) and (b) which show a negative bias for v and a non-symmetrical bias for T that is below 0.5. Studying the spanwise velocity fields at the two times shows an axial progression (not shown), i.e. the primarily upwelling velocity field that was at $x = 4.0$ at $t = 869.4$ has translated to $x = 5.0$ and has strengthened at the later time $t = 876.8$, etc.

Figures 11 and 12 show the temporal variations of

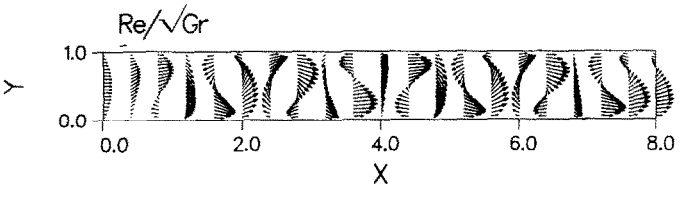

FIG. 9. Velocity field in the vertical central plane ($z = 1.0$) of the channel for $Re = 5$, $Gr = 5000$, $t = 270.6$.

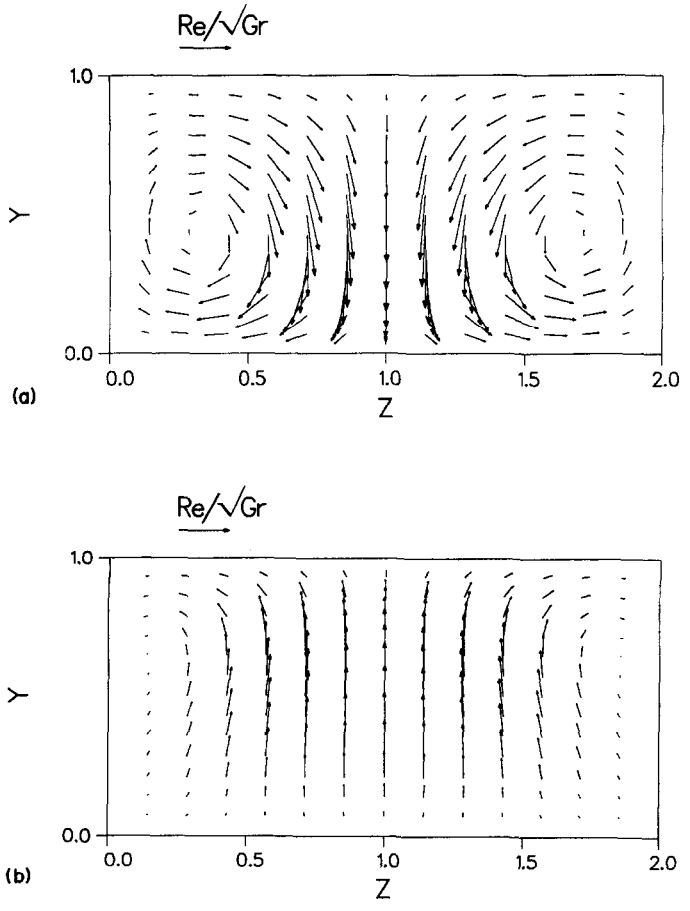

FIG. 10. Velocity fields in spanwise (yz) plane ($x = 5.0$) for $Re = 10$, $Gr = 5000$: (a) $t = 869.4$; (b) $t = 876.8$.

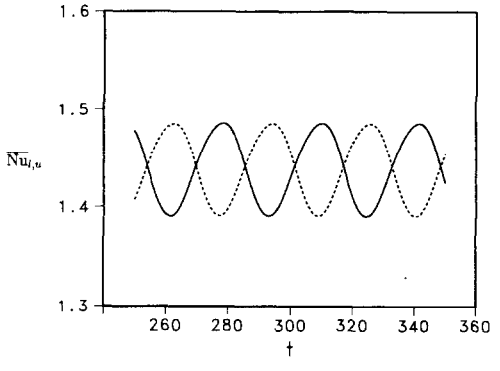

FIG. 11. Average Nusselt numbers on the lower hot surface (——) and the upper cold surface (– – –) of the channel for $Re = 5$, $Gr = 5000$.

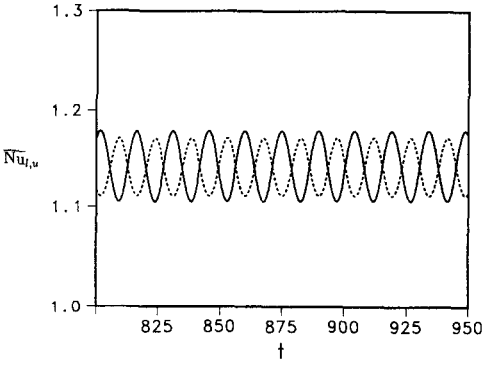

FIG. 12. Average Nusselt numbers on the lower hot surface (——) and the upper cold surface (– – –) of the channel for $Re = 10$, $Gr = 5000$.

the Nusselt numbers averaged over the bottom and top surfaces for $Re = 5$ and 10. The average Nusselt numbers are defined by

$$\overline{Nu}_{l,u} \equiv \frac{\overline{q^*_{l,u}} H}{k_0(T_s - T_0)} = \frac{H^2}{WL} \sum_{l,u} Nu_{l,u} \Delta x \Delta z. \quad (7)$$

The variation is periodic with constant amplitude and is related to the number of waves in the channel which varies with time. For $Re = 10$ the amplitude on the lower heated surface is larger than on the upper cooled surface although the time averaged values are the same (1.14). For $Re = 5$ the amplitudes on both surfaces are equal and the time averaged values are 1.44 on both surfaces.

Figure 13 shows the local Nusselt numbers for

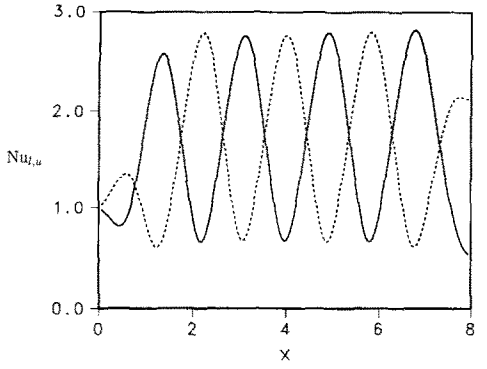

FIG. 13. Local Nusselt numbers on the lower hot surface (——) and the upper cold surface (– – –) along the central vertical plane ($z = 1.0$) of the channel at a time of maximum temperature at the center point, $(x, y, z) = (4.0, 0.5, 1.0)$, for $Re = 5$, $Gr = 5000$, $t = 270.6$.

$Re = 5$ on the lower and upper surfaces as a function of x along the center plane, $z = 1.0$, at $t = 270.6$. The local Nusselt numbers on the lower and upper surfaces of the channel are defined as

$$Nu_{l,u} \equiv \frac{q^*_{l,u} H}{k_0 (T_s - T_0)} = -k \frac{\partial \Theta}{\partial y}\bigg|_{y=0,1}. \tag{8}$$

Note that the local Nusselt numbers are defined in equation (8) to yield a value of unity when a linear temperature gradient, corresponding to heat conduction in a fluid with constant thermal conductivity, exists between the horizontal surfaces. At $x = 4.0$ the heat transfer is a local minimum on the lower surface and is a local maximum on the upper surface. This time corresponds to a maxima in both the temperature Θ and the vertical velocity v (cf. Figs. 2(a) and (b)) at the center point of the channel. In contrast, at $t = 286.4$ (not shown), at $x = 4.0$ the heat transfer is now a local maximum on the lower surface and it is a local minimum on the upper surface, corresponding to a minimum in temperature and strong downward flow (cf. Figs. 2(a) and (b)).

Figure 14 shows the local Nusselt numbers for $Re = 10$ on the lower and upper surfaces as a function of x along the center plane, $z = 1.0$, and $t = 869.4$. Similar trends to those discussed above for Fig. 13 are observed. Note that the heat transfer does not deviate from pure conduction until the instability begins near $x = 3$. The peak local heat flux in the unstable flow region is between 2.5 and 3 times greater than the value in the stable region $x < 3$, where the heat transfer is by conduction alone.

Figure 15 shows the local Nusselt numbers for $x = 4.0$ on the lower and upper surfaces as a function of spanwise coordinate z at $t = 270.6$ for $Re = 5$. As in the previous cases, this time corresponds to the occurrence of a maximum in Θ at the *center point*. Also recall that in Fig. 13 the *axial* variation of $Nu_{l,u}$ on the centerline ($z = 1.0$) at time $t = 270.6$ has a local minimum (on the lower surface) and maximum (on the upper surface) at $x = 4.0$. An exact reversal in $Nu_{l,u}$ (not shown) at this yz plane ($x = 4.0$) occurs at $t = 286.4$. At the center point this is consistent with the symmetric oscillations of temperature and vertical velocity discussed above; presumably these symmetric oscillations extend over the entire span in z.

Figures 16(a)–(d) show the spanwise (z) variation of the local Nusselt numbers for $x = 4.0$ and 6.0 on the lower and upper surfaces at $t = 869.4$ and 876.8 for $Re = 10$. Comparing $Nu_{l,u}$ at $x = 4.0$ (Fig. 16(a)) and 6.0 (Fig. 16(c)) at $t = 869.4$ shows both the increasing magnitude and the increasing spanwise variation that occurs as the instability becomes established further downstream in the channel (cf. Figs. 7(b) and 14). This trend of increased spanwise variation with increasing axial distance is markedly shown at the time $t = 876.8$ in Figs. 16(b) and (d). Also, comparing Figs. 16(a) and (b) shows a reversal as for $Re = 5$, but now the lack of symmetry in the oscillations (for Θ about 0.5 and for v about 0.0, cf. Figs. 4(a) and (b)) results in less than an exact reversal. Note that for $x = 4.0$ the two times displayed correspond to maxima and minima in temperature and vertical

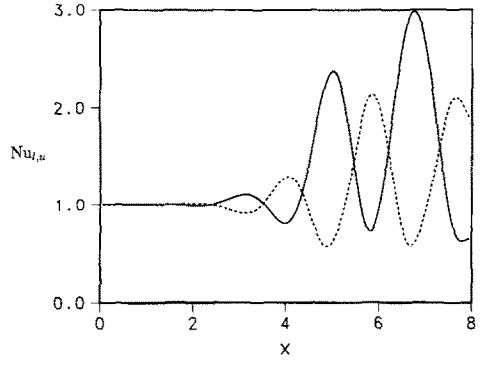

FIG. 14. Local Nusselt numbers on the lower hot surface (——) and the upper cold surface (– – –) along the central vertical plane ($z = 1.0$) of the channel at a time of maximum temperature at the center point, $(x, y, z) = (4.0, 0.5, 1.0)$, for $Re = 10$, $Gr = 5000$, $t = 869.4$.

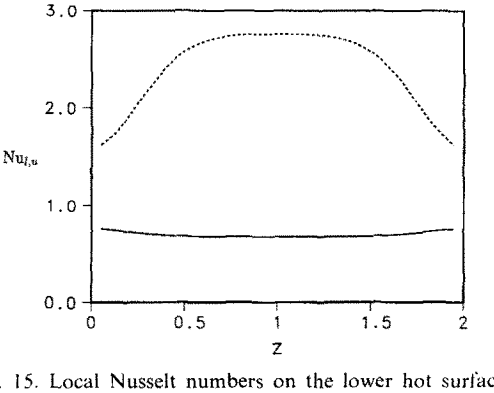

FIG. 15. Local Nusselt numbers on the lower hot surface (——) and the upper cold surface (– – –) along the spanwise (yz) plane ($x = 4.0$) of the channel at a time of maximum temperature at the center point, $(x, y, z) = (4.0, 0.5, 1.0)$, for $Re = 5$, $Gr = 5000$, $t = 270.6$.

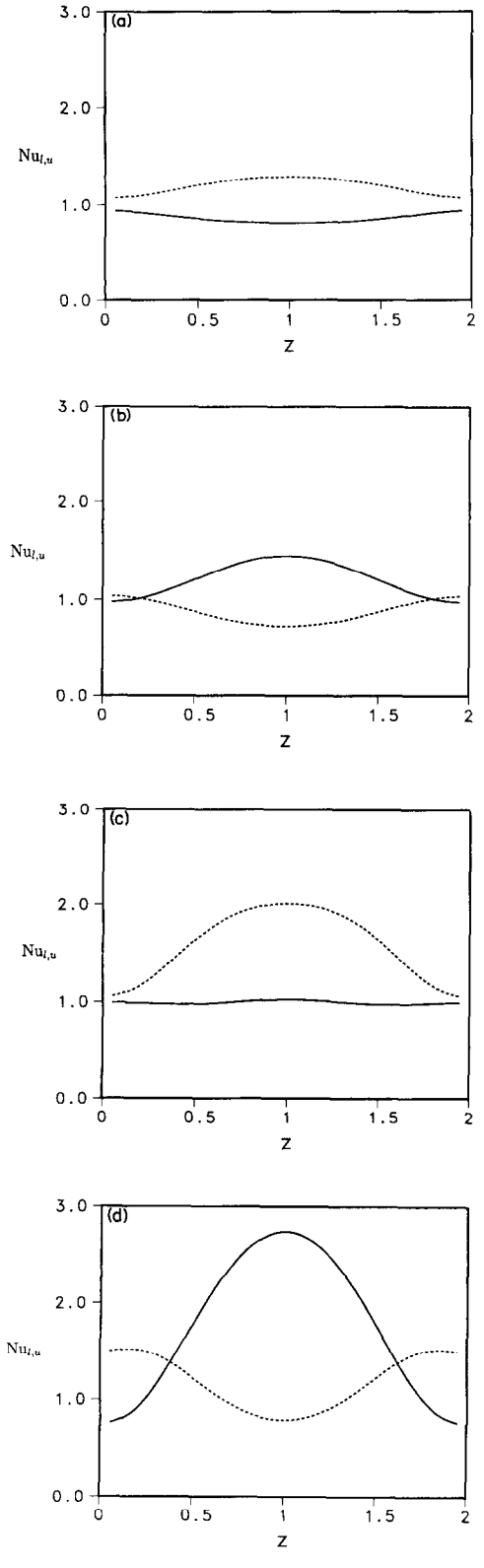

FIG. 16. Local Nusselt numbers on the lower hot surface (——) and the upper cold surface (– – –) along spanwise (yz) planes of the channel at times of maximum ($t = 869.4$) and minimum ($t = 876.8$) temperature at the center point, $(x, y, z) = (4.0, 0.5, 1.0)$, for $Re = 10$, $Gr = 5000$: (a) $x = 4.0$, $t = 869.4$; (b) $x = 4.0$, $t = 876.8$; (c) $x = 6.0$, $t = 869.4$; (d) $x = 6.0$, $t = 876.8$.

velocity at this position. Figures 16(c) and (d) ($x = 6.0$) also show an inexact reversal which is now much more pronounced than that shown in Figs. 16(a) and (b) at $x = 4.0$. This inexact reversal is due to both the lack of symmetry in the oscillations for Θ and v as noted above, as well as the fact that these times do not necessarily correspond to maxima and minima at the location $x = 6.0$.

For $t = 876.8$, at $x = 6.0$, the variation in heat transfer with spanwise coordinate z (cf. Fig. 16(d)) is large (similar in magnitude to the *axial* variation along the channel centerline). Note that the maximum heat transfer on the lower surface occurs in the central part of the channel but on the upper surface the maximum is near the side walls. This is further evidence of the spanwise recirculation discussed above which is beginning to have a large influence at 'large' x on the spanwise variation of the heat transfer.

In ref. [23] we studied the two-dimensional flow in a horizontal channel for conditions typical of CVD and observed transverse traveling waves. Since the $Gr = 5000$ with $Re = 5$ and 10 conditions were not discussed in ref. [23], we have performed these additional calculations of two-dimensional flow in a horizontal channel with $\varepsilon = 0.01$ and $L/H = 8.0$ to compare with the current three-dimensional results. For $Re = 10$, the two-dimensional results do not show an instability, suggesting that the side walls may be contributing to the instability for this condition. The destabilizing effect of adiabatic side walls at smaller values of W/H has recently been studied by Chou and Lin [27]. For $Re = 5$ the two-dimensional flow is unstable and the average Nusselt numbers are 10% larger and the frequency of the traveling waves is 32% greater than the three-dimensional results. Thus, for this condition the side walls appear to be damping the instability and reducing the heat transfer.

SUMMARY

We have predicted the unsteady, three-dimensional flow associated with the Rayleigh–Bénard thermal instability in a horizontal channel with a heated bottom surface and a cooled top surface. The velocity and temperature fields and the local and the average Nusselt numbers from the heated and cooled surfaces of the channel have been determined. The flow field and heat transfer are quite complex due to the interactions of traveling transverse waves, which sweep periodically through the channel, with longitudinal rolls, which results in significant recirculation in the spanwise direction, especially for $Re = 10$.

The comparison of these results with two-dimensional simulations shows complex effects of the side walls of the channel. For $Re = 10$, the side walls appear to contribute to the instability, whereas for $Re = 5$ the side walls appear to be damping the instability and reducing the heat transfer. Both two- and three-dimensional simulations show that the onset of thermal instability is delayed by increasing Re.

The heat transfer is increased considerably when the instability is present. For $Re = 5$, the average heat transfer is as much as 50% larger (the time average value is 44% larger) than the conduction values in fully developed horizontal channel flow, and for $Re = 10$ the peak local heat fluxes are three times larger than the fully developed flow values. For CVD applications the additional transfer resulting from the instability would significantly increase the deposition rate in the transport limited regime. Furthermore, since the instability results in a periodic flow condition, irregularities in the heat flux are smoothed out over time. However, careful control over the reactor operating parameters would be required to avoid flow conditions which result in the steady, longitudinal vortices that have been noted in some studies. These flow instabilities would yield striations in the deposited material. This study is of fundamental interest in respect to convective transport and should also help designers of CVD reactors gain a better understanding of the processes which occur in these systems.

Acknowledgement—Many helpful discussions with S. Paolucci, W. G. Breiland, M. E. Coltrin, A. W. Johnson and R. J. Kee are appreciated. This work was supported by the United States Department of Energy.

REFERENCES

1. K. F. Jensen, Modeling of chemical vapor deposition reactors, *Proc. 9th Int. Conf. on Chemical Vapor Deposition*, pp. 3–20 (1984).
2. L. J. Giling, Gas flow patterns in horizontal epitaxial reactor cells observed by interference holography, *J. Electrochem. Soc.* **129**(3), 634–644 (1982).
3. M. E. Coltrin, R. J. Kee and J. A. Miller, A mathematical model of the coupled fluid mechanics and chemical kinetics in a chemical vapor deposition reactor, *J. Electrochem. Soc.* **131**(2), 425–434 (1984).
4. S. Ostrach, Fluid mechanics in crystal growth—The 1982 Freeman Scholar Lecture, *J. Fluids Engng* **105**, 5–20 (1983).
5. B. J. Curtis and J. P. Dismukes, Effects of natural and forced convection in vapor phase growth systems, *J. Crystal Growth* **17**, 128–140 (1972).
6. R. Pollard and J. Newman, Silicon deposition on a rotating disk, *J. Electrochem. Soc.* **127**(3), 744–752 (1980).
7. M. E. Coltrin, R. J. Kee and G. H. Evans, A mathematical model of the fluid mechanics and gas-phase chemistry in a rotating-disk chemical vapor deposition reactor, *J. Electrochem. Soc.* **136**(3), 819–829 (1989).
8. G. W. Cullen (Editor), *Proc. Tenth Int. Conf. on Chemical Vapor Deposition*, pp. 11–32, 175–180, 193–203. The Electrochemical Society (1987).
9. H. Moffat and K. F. Jensen, Complex flow phenomena in MOCVD reactors, *J. Crystal Growth* **77**, 108–119 (1986).
10. H. Moffat and K. F. Jensen, Three-dimensional flow effects in silicon CVD in horizontal reactors, *J. Electrochem. Soc.* **135**(2), 459–471 (1988).
11. C. Houtman, D. B. Graves and K. F. Jensen, CVD in stagnation point flow, *J. Electrochem. Soc.* **133**(5), 961–970 (1986).
12. J. van de Ven, G. M. J. Rutten, M. J. Raaijmakers and L. J. Giling, Gas phase depletion and flow dynamics in horizontal MOCVD reactors, *J. Crystal Growth* **76**, 352–372 (1986).
13. Y. Mori and Y. Uchida, Forced convective heat transfer between horizontal flat plates, *Int. J. Heat Mass Transfer* **9**, 803–817 (1966).
14. K. S. Gage and W. H. Reid, The stability of thermally stratified plane Poiseuille flow, *J. Fluid Mech.* **33**(1), 21–32 (1968).
15. M. Akiyama, G. J. Hwang and K. C. Cheng, Experiments on the onset of longitudinal vortices in laminar forced convection between horizontal plates, *Trans. ASME J. Heat Transfer* 335–341 (November 1971).
16. S. Ostrach and Y. Kamotani, Heat transfer augmentation in laminar fully developed channel flow by means of heating from below, *Trans. ASME J. Heat Transfer* 220–225 (May 1975).
17. Y. Kamotani, S. Ostrach and Y. Miao, Convective heat transfer augmentation in thermal entrance regions by means of thermal instability, *Trans. ASME J. Heat Transfer* **101**, 222–226 (May 1979).
18. F. P. Incropera, A. L. Knox and J. R. Maughan, Mixed convection flow and heat transfer in the entry region of a horizontal rectangular duct, *Trans. ASME J. Heat Transfer* **109**, 434–439 (May 1987).
19. J. K. Platten and J. C. Legros, *Convection in Liquids*, Chap. 8. Springer, Berlin (1984).
20. J.-M. Luijkx, J. K. Platten and J. C. Legros, On the existence of thermoconvective rolls, transverse to a superimposed mean Poiseuille flow, *Int. J. Heat Mass Transfer* **24**, 1287–1291 (1981).
21. K. C. Chiu and F. Rosenberger, Mixed convection between horizontal plates—I. Entrance effects, *Int. J. Heat Mass Transfer* **30**, 1645–1654 (1987).
22. M. T. Ouazzani, J. P. Caltagirone, G. Meyer and A. Mojtabi, Etude numerique et experimentale de la convection mixte entre deux plans horizontaux a temperatures differentes, *Int. J. Heat Mass Transfer* **32**, 261–269 (1989).
23. G. Evans and R. Greif, A study of traveling wave instabilities in a horizontal channel flow with applications to chemical vapor deposition, *Int. J. Heat Mass Transfer* **32**, 895–911 (1989).
24. S. Paolucci, On the filtering of sound from the Navier Stokes equations, Sandia National Laboratories Report SAND82-8257 (1982).
25. A. D. Gosman and W. M. Pun, Calculation of recirculating flow, Lecture Notes, Imperial College of Science and Technology, London (1973).
26. S. V. Patankar, *Numerical Heat Transfer and Fluid Flow*. McGraw-Hill, New York (1980).
27. F. C. Chou and J. N. Lin, Convective instability in the thermal entrance region of horizontal rectangular channels, *Heat Transfer in Convective Flows, National Heat Transfer Conf.*, HTD-Vol. 107, pp. 329–336 (1989).

CONVECTION MIXTE TRIDIMENSIONNELLE VARIABLE DANS UN CANAL HORIZONTAL CHAUFFE AVEC APPLICATION A LA DEPOSITION CHIMIQUE DE VAPEUR

Résumé—On étudie l'écoulement et le transfert chimique d'un gaz dans un canal horizontal avec une surface inférieure chauffée, une surface supérieure refroidie et les parois latérales adiabatiques. Les solutions numériques des équations tridimensionnelles transitoires de Navier–Stokes et d'énergie révèlent que le fluide est instable thermiquement pour les conditions pratiques de la déposition chimique de vapeur (CVD). L'instabilité apparait comme la combinaison d'ondes progressives transverses et de rouleaux longitudinaux. La nature variable de l'écoulement et du transfert thermique est montrée pour deux nombres de Reynolds $Re = \bar{u}H/\nu_0$ (5 et 10), un nombre de Grashof $Gr = g\varepsilon H^3/\nu_0^2 = 5000$, un nombre de Prandtl $Pr = \nu_0/\alpha_0 = 2/3$, des rapports de forme $L/H = 8$ et $W/H = 2$, pour le rapport de température $\varepsilon = (T_s - T_0)/T_0 = 0{,}01$ et correspondant à des propriétés constantes du fluide. L'instabilité s'accompagne d'un accroissement du transfert thermique moyen entre 15% et plus de 40% par rapport à la condition d'écoulement établi sans instabilité.

NICHTSTATIONÄRE DREIDIMENSIONALE MISCHKONVEKTION IN EINEM BEHEIZTEN WAAGERECHTEN KANAL FÜR ANWENDUNGEN DER CHEMISCHEN DAMPFABSCHEIDUNG

Zusammenfassung—Es werden Strömung und Wärmeübertragung in einem Gas in einem waagerechten Kanal untersucht, dessen Oberfläche im unteren Teil beheizt, im oberen Teil gekühlt und an den Seiten adiabat ist. Numerische Lösungen der transienten dreidimensionalen Navier–Stokes-Gleichungen und der Energiegleichung zeigen eine thermische Instabilität des Fluids für die Bedingungen bei chemischer Dampfabscheidung. Die Instabilität zeigt sich als Kombination aus querverlaufenden Wanderwellen und längsverlaufenden Wirbeln. Die instationären Eigenschaften von Strömung und Wärmetransport werden für folgende Bedingungen gezeigt: Reynolds-Zahl $Re = \bar{u}H/\nu_0 = 5$ und 10, Grashof-Zahl $Gr = g\varepsilon H^3/\nu_0^2 = 5000$, Prandtl-Zahl $Pr = \nu_0/\alpha_0 = 2/3$, Seitenverhältnis $L/H = 8$ und $W/H = 2$, Temperaturverhältnis $\varepsilon = (T_s - T_0)/T_0 = 0{,}01$, entsprechend einer Strömung mit konstanten Eigenschaften. Die Instabilität führt zu einer Verbesserung des mittleren Wärmeübergangs zwischen 15% und mehr als 40% gegenüber dem Wert bei vollständig ausgebildeter Strömung ohne Instabilität.

НЕСТАЦИОНАРНАЯ ТРЕХМЕРНАЯ СМЕШАННАЯ КОНВЕКЦИЯ В НАГРЕТОМ ГОРИЗОНТАЛЬНОМ КАНАЛЕ ПРИ ХИМИЧЕСКОМ ОСАЖДЕНИИ ПАРА

Аннотация—Исследуются течение газа и теплоперенос в горизонтальном канале с нагреваемой нижней и охлаждаемой верхней поверхностями при адиабатических боковых стенках. Численные решения нестационарного трехмерного уравнения Навье–Стокса и уравнения энергии показывают, что в рассматриваемых условиях химического осаждения пара процесс является термически неустойчивым. Неустойчивость возникает в виде сочетания поперечных бегущих волн и продольных валов. Нестационарный характер течения и теплопереноса исследуется при двух значениях числа Рейнольдса $Re = \bar{u}H/\nu_0$ (5 и 10), значениях числа Грасгофа $Gr = g\varepsilon H^3/\nu_0^2 = 5000$, числа Прандтля $Pr = \nu_0/\alpha_0 = 2/3$, отношениях сторон $L/H = 8$ и $W/H = 2$ и отношении температур $\varepsilon = (T_s - T_0)/T_0 = 0{,}01$, при этом рассматривается течение с постоянными свойствами. Неустойчивость приводит к возрастанию теплопереноса в среднем от 15% до более чем 40% по сравнению с полностью развитым течением в отсутствие неустойчивости.